THE JOURNAL OF PHYSICAL CHEMISTRY A

Article

pubs.acs.org/JPCA

# Glyoxal Oxidation Mechanism: Implications for the Reactions HCO + $O_2$ and OCHCHO + $HO_2$

Nancy Faßheber,[†] Gernot Friedrichs,*[,†] Paul Marshall,[‡] and Peter Glarborg[§]

[†]Institute of Physical Chemistry, Christian-Albrechts-Universität Kiel, Max-Eyth-Str. 1, 24118 Kiel, Germany

[‡]Department of Chemistry and Center for Advanced Scientific Computing and Modeling (CASCaM), University of North Texas, 1155 Union Circle #305070, Denton, Texas 76203−5017, United States

[§]Department of Chemical and Biochemical Engineering, Technical University of Denmark, DK-2800 Kongens Lyngby, Denmark

Supporting Information

**ABSTRACT:** A detailed mechanism for the thermal decomposition and oxidation of the flame intermediate glyoxal (OCHCHO) has been assembled from available theoretical and experimental literature data. The modeling capabilities of this extensive mechanism have been tested by simulating experimental HCO profiles measured at intermediate and high temperatures in previous glyoxal photolysis and pyrolysis studies. Additionally, new experiments on glyoxal pyrolysis and oxidation have been performed with glyoxal and glyoxal/oxygen mixtures in Ar behind shock waves at temperatures of 1285−1760 K at two different total density ranges. HCO concentration−time profiles have been detected by frequency modulation spectroscopy at a wavelength of $\lambda$ = 614.752 nm. The temperature range of available direct rate constant data of the high-temperature key reaction HCO + $O_2$ → CO + $HO_2$ has been extended up to 1705 K and confirms a temperature dependence consistent with a dominating direct abstraction channel. Taking into account available literature data obtained at lower temperatures, the following rate constant expression is recommended over the temperature range 295 K < $T$ < 1705 K: $k_1/(\mathrm{cm^3\ mol^{-1}\ s^{-1}}) = 6.92 \times 10^6 \times T^{1.90} \times \exp(+5.73\ \mathrm{kJ/mol}/RT)$. At intermediate temperatures, the reaction OCHCHO + $HO_2$ becomes more important. A detailed reanalysis of previous experimental data as well as more recent theoretical predictions favor the formation of a recombination product in contrast to the formerly assumed dominating and fast OH-forming channel. Modeling results of the present study support the formation of HOCH(OO)CHO and provide a 2 orders of magnitude lower rate constant estimate for the OH channel. Hence, low-temperature generation of chain carriers has to be attributed to secondary reactions of HOCH(OO)CHO.

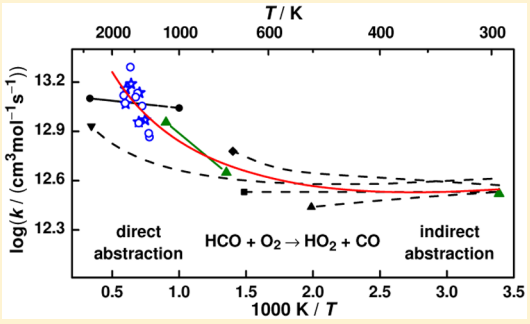


## INTRODUCTION

The oxidation chemistry of glyoxal (OCHCHO) is of interest, partly because it is recognized as an intermediate in combustion of hydrocarbons and partly because glyoxal has been identified as a promising HCO high-temperature source for shock tube measurements.[1,2] Moreover, glyoxal is discussed as an important component in tropospheric chemistry.[3,4] Glyoxal can be formed from oxidation of $C_2H_2$ at low to medium temperatures,[5−9] as well as in the atmosphere,[10−16] mostly through the chain-propagating sequence

$$C_2H_2 \xrightarrow{+OH} C_2H_2OH \xrightarrow{+O_2} OCHCHO + OH$$

Previous studies of OCHCHO chemistry include thermal decomposition in static reactors[17] and shock tubes[18,19] as well as low-temperature oxidation[20−22] and determination of explosion limits in static reactors.[23] Also, data on the low-temperature oxidation of glyoxal by $H_2O_2$[24] and $NO_2$[25] have been reported. More recently, Colberg and Friedrichs,[2] in a combined shock tube/photolysis study of OCHCHO/$O_2$ mixtures, obtained rate coefficients for the reaction HCO + $O_2$ at 750−1110 K. To our knowledge, no detailed chemical kinetic modeling studies of glyoxal oxidation have previously been reported.

The objective of the present study is 2-fold: We aim to develop a detailed chemical kinetic model for oxidation of OCHCHO in the intermediate to high temperature range for use in combustion studies. Furthermore, we wish to extend the measurement range for the rate constant of HCO + $O_2$ to higher temperatures. Novel shock tube experiments are conducted for OCHCHO and OCHCHO/$O_2$ mixtures in argon at temperatures from 1285 to 1760 K. The results from these experiments are combined with the previous data from Colberg and Friedrichs, and implications for our understanding

**Special Issue:** 100 Years of Combustion Kinetics at Argonne: A Festschrift for Lawrence B. Harding, Joe V. Michael, and Albert F. Wagner

**Received:** December 14, 2014
**Revised:** January 16, 2015
**Published:** January 22, 2015





DOI: 10.1021/jp512432q
J. Phys. Chem. A 2015, 119, 7305−7315

**Table 1. Thermodynamic Properties of Selected Species in the Reaction Mechanism[a]**

| species | $\Delta H^\circ_{298}$ | $S^\circ_{298}$ | $c_{p,300}$ | $c_{p,400}$ | $c_{p,500}$ | $c_{p,600}$ | $c_{p,800}$ | $c_{p,1000}$ | $c_{p,1500}$ | ref |
|---|---|---|---|---|---|---|---|---|---|---|
| OCHCHO | −212.07 | 272.45 | 60.60 | 71.38 | 81.42 | 89.93 | 101.43 | 108.64 | 117.36 | 30 |
| OCHCO | −63.80 | 281.28 | 57.81 | 65.15 | 71.39 | 76.64 | 84.65 | 90.17 | 98.25 | this work[b] |

[a]Units are kJ mol$^{-1}$ for $\Delta H$, J mol$^{-1}$ K$^{-1}$ for $S$ and $c_{p,T}$, and K for temperature $T$. [b]The C−H bond dissociation enthalpy at 298 K in OCHCHO was obtained via computed CBS-QB3 energies[31] and the reaction OCHCHO → OCHCO + H. There are isomers of OCHCO with bent C−C−O structures, but the most stable isomer has an almost linear C−C−O group. The corresponding bond dissociation enthalpy is 366.2 kJ mol$^{-1}$, which corresponds to $\Delta_f H^\circ_{298}$(OCHCO) = −63.8 kJ mol$^{-1}$. Entropies and heat capacities of OCHCO were derived using the harmonic oscillator/rigid rotor model.

**Table 2. OCHCHO Subset of the Reaction Mechanism[a]**

| no. | | $A$ [cm, mol, s] | $n$ | $E_a$ [kJ/mol] | ref |
|---|---|---|---|---|---|
| 1 | HCO + $O_2$ ⇌ CO + $HO_2$ | $6.9 \times 10^6$ | 1.900 | −5.73 | this work[b] |
| 2a | OCHCHO ⇌ $CH_2O$ + CO | $8.04 \times 10^{55}$ | −12.600 | 321.00 | 19[c] |
| 2b | OCHCHO ⇌ CO + CO + $H_2$ | $6.12 \times 10^{57}$ | −13.100 | 335.34 | 19[c] |
| 2c | OCHCHO ⇌ HCOH + CO | $2.62 \times 10^{57}$ | −13.200 | 333.69 | 19[c,d] |
| 2d | OCHCHO ⇌ HCO + HCO | $1.89 \times 10^{57}$ | −12.800 | 352.80 | 19[c] |
| 3 | OCHCHO + H ⇌ OCHCO + $H_2$ | $5.4 \times 10^{13}$ | 0 | 18.00 | 2 |
| 4 | OCHCHO + O ⇌ OCHCO + OH | $8.4 \times 10^{11}$ | 0.570 | 11.55 | est., 2 × $k_{CH_2O+O}$ |
| 5 | OCHCHO + OH ⇌ OCHCO + $H_2O$ | $4.0 \times 10^6$ | 2.000 | −6.82 | 32 |
| 6 | OCHCHO + $HO_2$ → HOCH(OO)CHO | $1.3 \times 10^{31}$ | −7.532 | 6.03 | 34[e] |
| −6 | HOCH(OO)CHO → OCHCHO + $HO_2$ | $1.9 \times 10^{29}$ | −5.781 | 66.07 | 34[e] |
| 7 | OCHCHO + $HO_2$ ⇌ HOCHO + CO + OH | $3.3 \times 10^{-4}$ | 3.995 | 1.26 | 34[e] |
| 8 | OCHCHO + $HO_2$ ⇌ OCHCO + $H_2O_2$ | $8.2 \times 10^4$ | 2.500 | 42.70 | est., 2 × $k_{CH_2O+HO_2}$ |
| 9 | OCHCHO + $O_2$ ⇌ OCHCO + $HO_2$ | $4.8 \times 10^5$ | 2.500 | 152.55 | est., 2 × $k_{CH_2O+O_2}$ |
| 10 | OCHCO ⇌ HCO + CO | $4.1 \times 10^{14}$ | 0 | 36.67 | 35[e] |
| 11a | OCHCO + $O_2$ ⇌ CO + $CO_2$ + OH | $3.3 \times 10^{14}$ | 0 | 8.68 | 35[e] |
| 12 | HOCH(OO)CHO → HOCHO + CO + OH | $1.6 \times 10^{10}$ | 0.051 | 63.56 | 34 |
| 13 | HOCH(OO)CHO + $HO_2$ → HOCH(O)CHO + $O_2$ + OH | $3.0 \times 10^{12}$ | 0 | 0 | est.[f,g] |
| 14 | HOCH(OO)CHO + $HO_2$ → HOCH(OOH)CHO + $O_2$ | $3.0 \times 10^{12}$ | 0 | 0 | est.[g] |

[a]Parameters for use in the modified Arrhenius expression $k = AT^n \exp(-E_a/RT)$. Units are mol, cm, s, kJ. The full mechanism, including pressure-dependent expressions, is given in the Supporting Information. [b]295 K < $T$ < 1705 K. [c]1.0 bar, 800 K < $T$ < 2500 K. [d]Treated as a duplicate of reaction (R2a), see text. [e]1.0 atm. [f]HOCH(O)CHO immediately dissociates to HOCHO and HCO. [g]298 K.

of glyoxal oxidation and for the overall rate constant of the reaction HCO + $O_2$ are discussed.

## DETAILED KINETIC MODEL

A mechanism has been assembled from recent work on the chemistry of glyoxal,[2,19] formic acid,[26] formaldehyde,[27] carbon monoxide,[28] and hydrogen.[29] In the present work, the OCHCHO oxidation subset of the mechanism was updated. The thermodynamic properties for OCHCHO and OCHCO are shown in Table 1,[30,31] whereas Table 2 lists key reactions in the OCHCHO oxidation scheme.[2,19,32,34,35] The full mechanism, including pressure-dependent rate coefficients for many decomposition and recombination reactions, is available as Supporting Information.

In addition to the OCHCHO subset discussed below, particular attention was paid to the reaction of HCO with $O_2$

$$\text{HCO} + \text{O}_2 \rightleftharpoons \text{CO} + \text{HO}_2 \qquad \text{(R1)}$$

High-temperature oxidation of hydrocarbons as well as of glyoxal is very sensitive to this step. Starting from the experimentally determined rate coefficients by Colberg and Friedrichs[2] and the new experimental data presented below, we derived a rate constant expression valid over a wide range of temperatures. Hsu et al.[36] reported a theoretical study of this reaction, based on RRKM calculations for the indirect abstraction channel and VTST calculations for the direct abstraction channel. Both channels yield the products CO + $HO_2$. According to these calculations, at low temperatures the more or less temperature-independent indirect channel dominates and the increase of the total rate constant, which is due to the direct abstraction channel, takes place not before temperatures of $T$ > 1250 K. In contrast, the Colberg and Friedrichs determination implies a distinct increase of the rate constant already at temperatures above $T$ > 700 K. For the temperature range of the present shock tube study (1285−1705 K), the extrapolated Arrhenius expression of Colberg and Friedrichs yields 2.1−2.5 times higher values than the theoretical prediction of Hsu et al. Hence, the new glyoxal oxidation experiments served as a critical test of both the absolute value of the rate constant and the overall temperature dependence of the reaction HCO + $O_2$.

Thermal dissociation of OCHCHO has been characterized experimentally behind shock waves[18,19] and theoretically.[19,37] It


DOI: 10.1021/jp512432q
J. Phys. Chem. A 2015, 119, 7305−7315

is a highly temperature- and pressure-dependent multichannel reaction that may yield a range of products

$$OCHCHO \rightleftharpoons CH_2O + CO \quad (R2a)$$

$$OCHCHO \rightleftharpoons CO + CO + H_2 \quad (R2b)$$

$$OCHCHO \rightleftharpoons HCOH + CO \quad (R2c)$$

$$OCHCHO \rightleftharpoons HCO + HCO \quad (R2d)$$

We have adopted the results by Friedrichs et al.,[19] who detected species profiles of OCHCHO, HCO, and H behind shock waves at temperatures of 1032−2320 K. In their work, the obtained branching ratios of the thermal glyoxal decomposition were interpreted by means of RRKM/SACM/ME calculations, and rate coefficients over a wide range of temperatures (800−2500 K) and pressures (1 mbar to 100 bar) have been reported. Original data have been represented in terms of Chebyshev polynomial coefficients. We reparametrized their data and report extended Arrhenius expressions at $p$ = 1 bar in Table 2 and at other total pressures in the Supporting Information. A key finding of Friedrichs et al. was that the previously neglected, energetically most unfavorable HCO channel (R2d), due to its loose transition state character, becomes the dominant product channel at high temperatures and pressures. For example, at $T$ = 2300 K and $p$ = 3 bar, the branching fraction of channel (R2d) accounts for 48% of the total reaction rate. In contrast, the hydroxymethylene forming HCOH channel (R2c), in agreement with a photochemical study of Hepburn et al.,[38] with branching fractions <7% at all temperatures and pressures turned out to be minor. Arguments have been put forward in ref 19 that subsequent chemistry of HCOH is not expected to serve as a significant source of additional atoms or radicals such that the overall influence of this minor channel on glyoxal chemistry remains small. With regard to a simplified description of the thermal decomposition of glyoxal, channel (R2c) has, therefore, not been treated as a separate channel, but its reported rate constant expression has been merged with reaction channel (R2a), which is the main channel under the experimental conditions of this work.

Other reactions of OCHCHO include abstraction of H by radicals or $O_2$. Only a few of these steps have been characterized experimentally. The reaction with atomic hydrogen (R3)

$$OCHCHO + H \rightleftharpoons OCHCO + H_2 \quad (R3)$$

has been measured at elevated temperatures (769−1107 K) by Colberg and Friedrichs,[2] and their value is used in the reaction mechanism. The reaction with OH (R5)

$$OCHCHO + OH \rightleftharpoons OCHCO + H_2O \quad (R5)$$

has been studied both experimentally[32,33,39] and theoretically,[40] although only at low temperatures. The experimental results are in good agreement. We have adopted the rate constant measured by Feierabend et al.[32] in the 210−390 K range.

For the reactions of OCHCHO with O (R4) and $O_2$ (R9)

$$OCHCHO + O \rightleftharpoons OCHCO + OH \quad (R4)$$

$$OCHCHO + O_2 \rightleftharpoons OCHCO + HO_2 \quad (R9)$$

we estimate the rate constants to be similar to the analogue reactions of $CH_2O$.

The reaction of OCHCHO with $HO_2$ is of particular importance because $HO_2$ is formed in significant quantities compared to the other radicals in the O/H pool under low to medium temperature conditions. The H-abstraction channel

$$OCHCHO + HO_2 \rightleftharpoons OCHCO + H_2O_2 \quad (R8)$$

has not been characterized experimentally, but we assume that it has a rate constant similar to that of $CH_2O + HO_2$. The reaction would be expected to be too slow to compete at low temperatures, but it may become dominating at elevated temperatures. According to the recent theoretical study of da Silva,[34] the main product of OCHCHO + $HO_2$ at low temperature is HOCH(OO)CHO

$$OCHCHO + HO_2 \rightleftharpoons HOCH(OO)CHO \quad (R6)$$

However, even at low temperatures, the HOCH(OO)CHO radical predominantly dissociates to reform the reactants.[34] In analogy with a corresponding formaldehyde reaction

$$CH_2O + HO_2 \rightleftharpoons HOCHO + OH$$

a secondary product channel yielding OH radicals has been proposed for glyoxal oxidation by Hay and Norrish[21]

$$OCHCHO + HO_2 \rightleftharpoons OCHC(O)OH + OH$$

OCHC(O)OH would be expected to decompose rapidly to formic acid (HOCHO) + CO. Indeed, the existence of the OH-producing channel for glyoxal + $HO_2$ seems to be supported by the detection of formic acid[41] in glyoxal oxidation and appears to be required to explain the generation of chain carriers in glyoxal oxidation at 563−643 K.[21] From a photolysis study at 298 K, Niki et al.[41] derived a room-temperature value for the OH channel of $3 \times 10^8$ cm$^3$ mol$^{-1}$ s$^{-1}$. Support for an OH-producing channel of the OCHCHO + $HO_2$ reaction is also provided theoretically. According to da Silva,[34] the reaction forms a hydroxyperoxy radical, which decomposes to HOCHO + CO + OH

$$OCHCHO + HO_2 \rightarrow HOCHO + CO + OH \quad (R7)$$

However, the rate constant calculated by da Silva is 2 orders of magnitude smaller than the value reported by Niki et al. In order to resolve this discrepancy, we have thoroughly reinterpreted the experimental results of Niki et al. (see Appendix). Our analysis indicates that the data of Niki et al. are compatible with the rate constant for (R7) from da Silva,[34] provided that the association reaction (R6) and the subsequent reactions of HOCH(OO)CHO are taken into account. Consequently, we have adopted the rate coefficients for (R6) and (R7) from da Silva.

Only a few studies of the chemistry of the OCHCO radical have been reported.[33,41,42] It is expected to decompose thermally or react with $O_2$. The thermal dissociation

$$OCHCO \rightleftharpoons HCO + CO \quad (R10)$$

was studied theoretically by da Silva,[35] who determined a high-pressure limit of $k_{10,\infty}/s^{-1} = 1.1 \times 10^{14} \times T^{0.133} \times \exp(-5102/T)$ between 200 and 2000 K. Under the conditions of interest in the present study, this reaction is in the fall-off regime, and consequently we used extrapolations of rate constants provided by da Silva for the 150−400 K range for pressures of 0.01, 0.1, and 1 atm. The rate constant calculated by da Silva is considerably lower than the experimental value reported by Orlando and Tyndall[42] for 0.92 atm and 224−370 K. However, the latter determination was affected by the use of a too large rate constant value for OCHCO + $O_2$, as pointed out by da Silva.[35]



DOI: 10.1021/jp512432q
J. Phys. Chem. A 2015, 119, 7305−7315

**Table 3. Experimental Conditions and Results**

| without $O_2$ | | | with $O_2$ | | | | |
|---|---|---|---|---|---|---|---|
| $T$/K | $\rho/10^{-6}$ mol cm$^{-3}$ | $x$(glyoxal) % | $T$/K | $\rho/10^{-6}$ mol cm$^{-3}$ | $x$(glyoxal) % | $x(O_2)$ ppm | $k_1/10^{12}$ cm$^3$ mol$^{-1}$s$^{-1}$ |
| | Incident Shock Wave | | | | Incident Shock Wave | | |
| 1299 | 3.87 | 1.01 | 1285 | 3.86 | 1.01 | 3185 | 7.3 |
| 1379 | 5.24 | 1.04 | 1294 | 3.86 | 1.01 | 6700 | 7.7 |
| 1398 | 3.94 | 1.01 | 1382 | 3.93 | 1.01 | 3185 | 11.3 |
| 1406 | 4.60 | 1.14 | 1432 | 3.96 | 1.01 | 6700 | 8.9 |
| 1466 | 3.98 | 1.01 | 1450 | 5.30 | 1.04 | 9415 | 13.6 |
| 1521 | 5.35 | 1.04 | 1481 | 4.66 | 1.14 | 7210 | 12.9 |
| 1757 | 3.95 | 1.01 | 1572 | 5.39 | 1.04 | 9415 | 19.6 |
| | | | 1677 | 4.09 | 1.01 | 6700 | 11.8 |
| | | | 1705 | 4.07 | 1.01 | 3185 | 13.2 |
| | Reflected Shock Wave | | | | Reflected Shock Wave | | |
| 1382 | 9.80 | 1.05 | 1339 | 9.61 | 1.05 | 5045 | 9.3 |
| 1519 | 10.3 | 1.05 | 1340 | 10.0 | 1.05 | 7735 | 9.3 |
| 1539 | 10.4 | 1.05 | 1420 | 9.96 | 1.05 | 5045 | 13.7 |
| 1545 | 11.6 | 1.01 | 1431 | 10.0 | 1.04 | 7645 | 9.1 |
| 1618 | 10.7 | 1.05 | 1558 | 11.6 | 1.02 | 4880 | 15.5 |
| | | | 1660 | 10.8 | 1.05 | 9060 | 14.4 |
| | | | 1663 | 10.8 | 1.05 | 7735 | 11.7 |

The reaction of OCHCO with $O_2$ could involve a number of product channels, i.e.

$$OCHCO + O_2 \rightleftharpoons CO + CO_2 + OH \quad (R11a)$$

$$OCHCO + O_2 \rightleftharpoons CO + CO + HO_2 \quad (R11b)$$

$$OCHCO + O_2(+M) \rightleftharpoons OCHC(O)OO(+M) \quad (R11c)$$

da Silva[35] predicts the CO + $CO_2$ + OH channel (R11a) to be dominating above room temperature. In fact, in a recent kinetic study on OH formation in the Cl/OCHCHO/$O_2$ reaction system, Lockhart et al.[33] found strong evidence that the reaction (R11) directly yields OH radicals with a rate constant consistent with the da Silva estimate. The OCHCO + $O_2$ addition reaction is strongly exothermal, and isomerization/decomposition of the excited peroxy radical adduct is competitive with collisional deactivation even at low temperature, leading directly to the dissociated products $CO_2$ + CO + OH. Similar to reaction (R10), da Silva uses RRKM/ME theory to calculate values of $k_{11a}$ for temperatures between 150 and 400 K and pressures of 0.01−1 bar; we extrapolate these data to the conditions of the present work. The work of da Silva indicates a small, positive activation energy (4−8 kJ mol$^{-1}$). The finding that (R11a) is the main product channel for OCHCO + $O_2$ is in agreement with experimental observations by Orlando and Tyndall.[42] However, they assumed the reaction to be barrierless and estimated a somewhat larger rate constant.

Addition of $O_2$ (R11c) yields a ketoperoxy radical, OCHC(O)OO. This radical isomerizes with a computed barrier of 63 kJ mol$^{-1}$ to make OCC(O)OOH through a 1−4 hydrogen shift. With a low barrier of 28 kJ mol$^{-1}$, the OCC(O)OOH radical would dissociate fast to form CO + $CO_2$ + OH, an overall step equivalent to (R11a). Alternatively, the ketoperoxy radical could pick up an H atom at the radical oxygen, resulting in OCHC(O)OOH. The new O−H bond with a bond energy of 407 kJ mol$^{-1}$ is reasonably strong; thus, H might be abstracted from other species present, including glyoxal. OCHC(O)OOH can decompose in a unimolecular step with a barrier of 87 kJ mol$^{-1}$ to yield HCO + $CO_2$ + OH, or it can be converted to OCC(O)OOH by abstraction of H from the C−H bond. With a bond energy of 379 kJ mol$^{-1}$, this bond is weaker than the O−H bond. However, da Silva predicts the association rate (R11c) to decrease rapidly above 300 K, and these pathways are not expected to be important under the conditions of the present study.

## EXPERIMENTAL SECTION

The thermal decomposition of glyoxal has been investigated behind shock waves with and without oxygen present in the reaction gas mixtures. All experiments were carried out in an electropolished stainless steel shock tube that is described in detail elsewhere.[2] The shock tube has been operated using hydrogen or hydrogen/nitrogen mixtures as driver gas and a 30 or 80 $\mu$m thick aluminum diaphragm. Concentration−time profiles of the glyoxal decomposition product HCO were measured by means of frequency modulation (FM) spectroscopy at a detection wavelength of $\lambda$ = 614.752 nm. The experimental setup was very similar to the one used in our previous paper on the reaction HCO + $O_2$.[2] Details on the HCO detection scheme and the implementation of FM spectroscopy for quantitative measurements of radicals behind shock waves can be found elsewhere.[43,44] According to FM theory, the measured signal $I_{FM}$ is related to the absolute radical concentration $c$ by the equation

$$I_{FM} = \frac{I_0}{2}\sigma_c c l \times \Delta f \times G$$

Here, $I_0$ is the probe light intensity, $\sigma_c$ is the absorption cross-section at line center, and $l$ is the absorption path length. $\Delta f$, the so-called FM factor, depends on the applied modulation frequency as well as the modulation depth and is calculated from the absorption line shape profile at the actual experimental temperature and pressure. Accurate line shape data and absorption cross-sections have been adopted from Friedrichs et al.[43] The room-temperature value of the absorption cross-section is in excellent agreement (within 2%) with the accurate measurements of Flad et al.[45] Allowance was made for a small pressure broadening effect according to an assumed pressure broadening coefficient $\Delta\nu = 2.0 \times (T/298\ K)^{0.75}$ GHz bar$^{-1}$, which is similar to the one experimentally



DOI: 10.1021/jp512432q
J. Phys. Chem. A 2015, 119, 7305−7315

Table 4. Previously Reported Channel Branching Ratios and Total Rate Constants of the Multichannel Thermal Decomposition of Glyoxal for Typical Experimental Conditions Behind the Incident ($\rho = 4.43 \times 10^{-6}$ mol cm$^{-3}$) and Reflected ($\rho = 1.05 \times 10^{-5}$ mol cm$^{-3}$) Shock Waves[a]

| OCHCHO → products | $T$ = 1300 K | | $T$ = 1700 K | |
|---|---|---|---|---|
| $\rho$/(mol cm$^{-3}$) | $1.05 \times 10^{-5}$ | $4.43 \times 10^{-6}$ | $1.05 \times 10^{-5}$ | $4.43 \times 10^{-6}$ |
| $\phi$ ($CH_2O$ + CO) % | 48 | 56 | 38 | 47 |
| $\phi$ (2 CO + $H_2$) % | 29 | 28 | 27 | 29 |
| $\phi$ (HCOH + CO) % | 7 | 7 | 6 | 7 |
| $\phi$ (2 HCO) % | 16 | 9 | 29 | 17 |
| $k_{2,\mathrm{total}}$/s$^{-1}$ | $1.3 \times 10^4$ | $8.3 \times 10^3$ | $7.1 \times 10^5$ | $3.8 \times 10^5$ |

[a]According to Friedrichs et al.[19]

observed for $NH_2$.[46] $G$ is the device-specific electronic gain factor of the FM spectrometer, which has to be determined separately. Its value has been remeasured and was found to be consistent with our previous determinations. We estimate the accuracy of the calculated HCO concentrations (including the error of the gain factor and the high-temperature extrapolation of the HCO cross-section) to be ±20%.

Glyoxal was prepared by heating glyoxal trimeric dihydrate in the presence of $P_2O_5$ and was stored in a liquid nitrogen trap. Reaction gas mixtures were prepared manometrically and contained 1% glyoxal in argon. Such high glyoxal mole fractions were necessary to ensure detectable HCO concentration levels. In about half of the experiments, mole fractions of 3185−9415 ppm oxygen have been added using a flow system with mass flow controllers. Experiments have been performed behind incident (corresponding to an average total density $\rho \approx 4.4 \times 10^{-6}$ mol cm$^{-3}$) and reflected ($\rho \approx 1.1 \times 10^{-5}$ mol cm$^{-3}$) shock waves in the temperature range 1299 K < $T$ < 1757 K. The experimental conditions of all 28 shock tube experiments, as calculated from the measured shock wave velocity and preshock conditions using a standard shock tube code with real gas correction, are outlined in Table 3. It is known that the vibrational relaxation/equilibration of oxygen is quite slow, about 100 $\mu$s at $T$ = 1500 K and $p$ = 1 bar in argon.[47] Therefore, in contrast to the translational and rotational degrees of freedom that are heated within 1 $\mu$s, the vibrational degrees of freedom are not in thermal equilibrium on the typical experimental time scales of 7−70 $\mu$s present in this study. This has two consequences: On the one hand, the real initial temperatures behind the shock waves were somewhat higher than calculated by the standard shock tube code. Therefore, Table 3 lists a corrected, up to 10 K higher, initial temperature assuming that the $O_2$ vibrational degree of freedom is not heated at all. On the other hand, as the actual $O_2(v = 1)/O_2(v = 0)$ ratio during the experiment is lower than at thermal equilibrium (about 0.2 at $T$ = 1400 K), the determined rate constant may be slightly biased by the different reactivities of $O_2$ in its $v$ = 0 and $v$ = 1 vibrational states. This nonequilibrium effect is difficult to address quantitatively and is typically neglected in the analysis of shock tube data. Within the scatter of the obtained rate constant data and taking into account the very good agreement with our previous shock tube measurements (which were not affected due to a sufficiently long delay behind the shock wave arrival and glyoxal photolysis), we assume that the possible, presumably negative, bias is not significant.

## RESULTS AND DISCUSSION

**Branching Ratio of Glyoxal Decomposition.** Experiments with glyoxal/argon mixtures without oxygen were performed to test the overall thermal glyoxal decomposition mechanism reported in the literature. According to Friedrichs et al.,[19] the channel branching of the multichannel unimolecular decomposition of glyoxal is strongly dependent on the temperature and total density. The effect of total density and temperature on the channel branching ratio is illustrated in Table 4. Note the pronounced fall-off of the total rate constant $k_{2,\mathrm{total}}$ ($\rho^{\mathrm{reflected}}/\rho^{\mathrm{incident}} = 2.5$, but $k_{2,\mathrm{total}}^{\mathrm{reflected}}/k_{2,\mathrm{total}}^{\mathrm{incident}} \approx 1.7$) and the significantly different importance of the HCO channel (R2d) at the two different temperatures ($\phi_{1700\mathrm{K}}/\phi_{1300\mathrm{K}} \approx 1.8$). Hence, the experiments behind the incident and reflected shock waves at overall different total densities provide a critical test of their rate constant data and RRKM/SACM/ME predictions.

Experimental HCO concentration−time profiles behind the reflected shock wave at three different temperatures are shown in Figure 1a together with simulated profiles (thick curves). Figure 1b illustrates the corresponding sensitivity analysis of the $T$ = 1519 K experiment in order to identify the most important reactions. The numerical simulations were performed using the CHEMKIN-II package[48] and the SENKIN routine[49] based on the glyoxal oxidation mechanism outline above. Overall, the observation times of the HCO profiles were rather short, and the initial increase of the HCO profiles were obscured by the strong Schlieren signal attributable to the passage of the shock wave through the detection laser beam. For a better comparison of the experimental and numerically simulated profiles, the experimental time resolution has been taken into account by convoluting the numerical simulation with an appropriate time response function (Gaussian, FWHM of 2−3 $\mu$s). Excluding the first few microseconds that are affected by the Schlieren signal (open symbols), both the absolute concentrations and the overall shapes of the reported concentration−time profiles are very well-captured by the simulations. Toward low temperatures, the experimentally accessible temperature range was limited by too low intermediate concentrations, and toward high temperatures, by too short HCO lifetimes. The sensitivity analysis in Figure 1b highlights the influence of the five most important reactions. Both the branching ratio of the OCHCHO decomposition and the rate constant of several secondary reactions have to be known to accurately predict the HCO profile. In fact, we were able to reproduce all measured HCO profiles without adjusting any rate constant data, initial glyoxal concentrations, or the temperature-dependent HCO absorption cross-section. From this high reproducibility, we conclude


DOI: 10.1021/jp512432q
J. Phys. Chem. A 2015, 119, 7305−7315

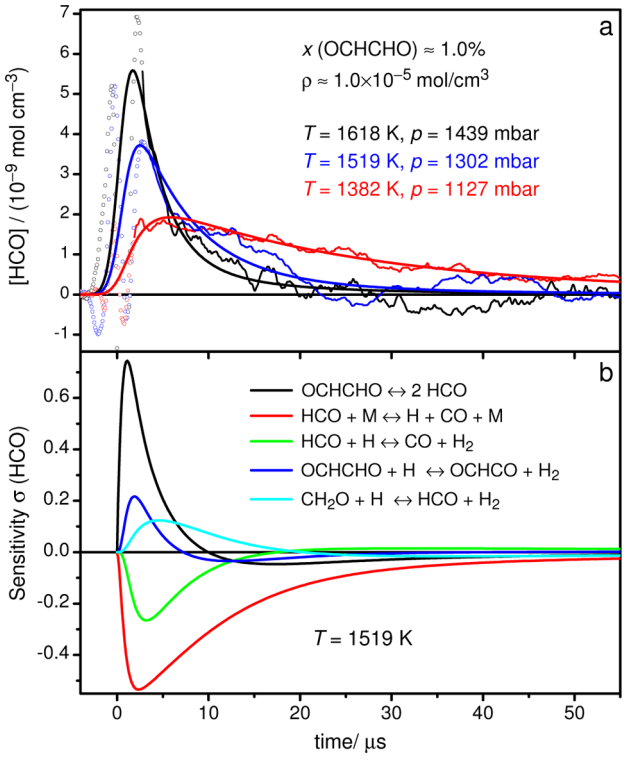


**Figure 1.** (a) Three experimental HCO profiles at different temperatures behind reflected shock waves in comparison with numerically simulated profiles. Open circles mark the interfering Schlieren signals and do not contain information on HCO concentration. (b) Corresponding HCO sensitivity analysis for $T$ = 1519 K. The sensitivity coefficients are normalized with respect to the maximum HCO concentration over the time history, $\sigma(\mathrm{HCO}) = 1/[\mathrm{HCO}]_{max} \times \partial[\mathrm{HCO}](t)/\partial \ln k$).

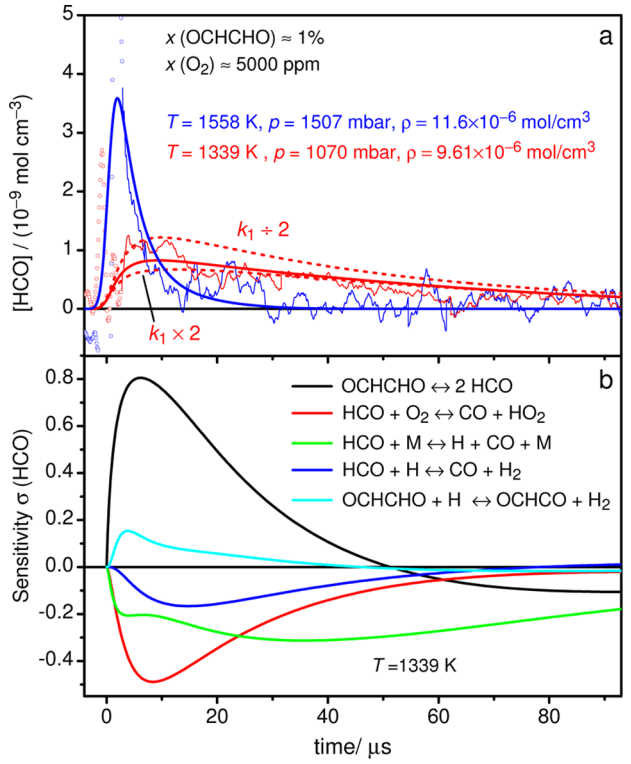


**Figure 2.** (a) Two typical experimental HCO concentration−time profiles in comparison with simulations (thick curves). The simulated profiles have been convoluted with an appropriate response function in order to allow for a direct comparison of the experiment and simulation at short reaction times. Open circles mark the interfering Schlieren signals, which were excluded from the fit. (b) Corresponding HCO sensitivity analysis for the experiment at $T$ = 1339 K. Only the five most sensitive reactions are shown.

that both the thermal glyoxal decomposition mechanism and the HCO detection scheme are highly reliable.

**Rate of Reaction HCO + $O_2$.** The rate constant of the reaction

$$\mathrm{HCO} + \mathrm{O_2} \rightarrow \mathrm{CO} + \mathrm{HO_2} \qquad \text{(R1)}$$

has been measured between 1285 K ≤ $T$ ≤ 1705 K at two different total densities of $\varrho \approx 4.3 \times 10^{-6}$ mol cm$^{-3}$ behind the incident and $\varrho \approx 1.0 \times 10^{-5}$ mol cm$^{-3}$ behind the reflected shock waves. The experimental conditions and the results for $k_1$ are summarized in Table 3. Next to 1% glyoxal, serving as a source of HCO radicals from reaction (R2d), the reaction mixtures contained 3185−9415 ppm of $O_2$. Figure 2a illustrates two typical experimental HCO concentration−time profiles measured behind reflected shock waves at a temperature of 1339 and 1558 K, respectively. Both experiments were carried out at similar densities ($\varrho$ = 1.16 and 0.96 × 10$^{-6}$ mol cm$^{-3}$) and initial glyoxal (1.02 and 1.05%) and $O_2$ mole fractions (4880 and 5045 ppm). The observed peak HCO concentration is about 4 times lower at the lower temperature. For the 1558 K experiment, the total HCO observation time is only about 40 $\mu$s, whereas HCO could be observed for >200 $\mu$s at 1339 K. This behavior is well-captured by the two simulated profiles (thick curves) using our glyoxal oxidation mechanism. Figure 2b illustrates the results of the sensitivity analysis of the $T$ = 1339 $K$ experiment. It reveals that the simulated absolute concentration levels are mainly determined by the branching ratio of the thermal decomposition of glyoxal, in particular the rate constants of the reaction (R2b), and by the assumed rate constant for the target reaction (R1). Other consecutive reactions of HCO and glyoxal are also important, but their rates have been validated together with the branching ratio by the shock tube measurements for mixtures without $O_2$ as outlined above. Hence, it was possible to obtain a best-fit value for the rate constant of the reaction HCO + $O_2$ by adjusting exclusively $k_1$. The two dashed curves in Figure 2a, corresponding to numerical simulations with $k_1$ set to $k_1$ × 2 and $k_1$/2, demonstrate the sensitivity of this procedure. Especially with respect to the HCO peak concentration, the effect of changing $k_1$ is very pronounced. Nevertheless, due to the moderate signal-to-noise ratio of the experiments, we estimate that the uncertainty of each individual $k_1$ value with ±75% is rather large.

The obtained $k_1$ values are depicted as red symbols in comparison with selected literature data in the Arrhenius plot shown in Figure 3. The included red error bar corresponds to the ±75% uncertainty of a single data point; the 2$\sigma$ standard deviation of the data with respect to the final Arrhenius fit (red curve) is about ±40%. For a more complete comparison of available literature data and a critical assessment of available room temperature data we refer to our previous publication[2] and the paper of DeSain et al.[50] Within the scatter of the data, the experiments behind the incident (open circles) and reflected shock waves (star symbols) are consistent; hence, no dependence of the rate constant on the total density could be identified. In contrast, a weak positive temperature


DOI: 10.1021/jp512432q
J. Phys. Chem. A 2015, 119, 7305−7315

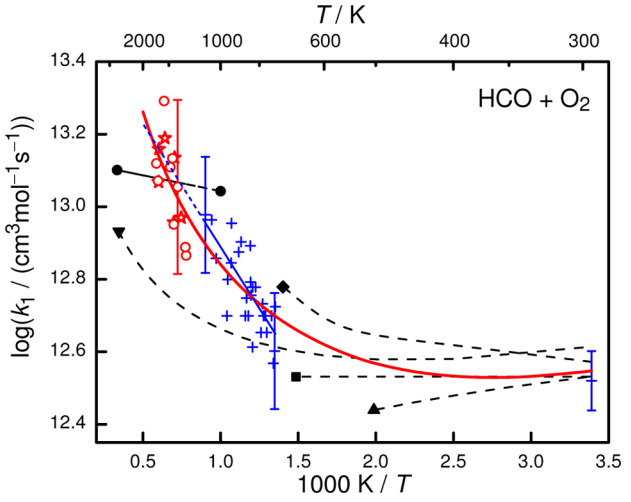


**Figure 3.** Arrhenius plot of the measured rate constants $k_1$ for the reaction HCO + $O_2$ of this work (incident wave, ○; reflected wave, ☆) in comparison with selected experimental data from Colberg and Friedrichs (+, blue line),[2] Veyret and Lesclaux (▲),[52] Timonen et al. (◆),[53] DeSain et al. (■),[50] the GRI-Mech 3.0 recommendation (●),[51] and the theoretical study of Hsu et al. (▼).[36] The red curve depicts the final recommended $k_1$ rate expression.

dependence is evident. Both the temperature dependence and the absolute rate constant values are in quantitative agreement with the high-temperature extrapolation (blue dashed line) of our previous determination[2]

$$k_1/(\mathrm{cm^3\,mol^{-1}\,s^{-1}}) = 3.7 \times 10^{13} \times \exp(-13\ \mathrm{kJ/mol}/RT)$$

The original data and error bars of the latter study are included as blue plus symbols. They had been determined using the 193 nm photolysis of glyoxal as a source of HCO radicals, and their uncertainty, unlike the uncertainty of the experiments in this work, was mainly due to the assumed initial ratio of [H]/[HCO] from glyoxal photolysis. The very good agreement of these two independent studies points out the consistent modeling capabilities of our mechanism with regard to glyoxal photolysis and pyrolysis.

The recommended value from the GRI-Mech. 3.0[51] (line marked with black filled circles) is in agreement with the new high-temperature results, but the temperature dependence is quite underestimated. The RRKM/VTST calculations of Hsu et al.[36] (curve marked with down triangle) underpredict the onset of the high-temperature direct abstraction channel, resulting in about 2 times lower absolute $k_1$ values at temperatures around 1500 K. Other experimental data for intermediate temperatures and at room temperature[2,50,52,53] reveal a more or less temperature-independent rate constant, which is consistent with the expected capture controlled process of the indirect abstraction channel with an initiating recombination step and a low-lying exit barrier to the products CO + $HO_2$. As a reasonable fit of the overall temperature dependence of the available data, an extended Arrhenius expression is recommended over the temperature range 295 K < $T$ < 1705 K (red curve)

$$k_1/(\mathrm{cm^3\,mol^{-1}\,s^{-1}}) = 6.92 \times 10^6 \times T^{1.90} \times \exp(+5.73\ \mathrm{kJ/mol}/RT)$$

The overall rate constant is independent of pressure. Even at room temperature, the collisionally deactivated recombination product $HC(O)O_2$ does not play a role provided that the pressure does not exceed several bar.[36]

**Model Validation against Literature Data.** To test the capacity of our mechanism, we used it for the modeling of other available experimental literature data. In particular, the batch reactor experiments of Hay and Norrish[21] were of interest. Their study, which was based on manometric detection of the reaction progress and gas chromatographic product analysis, should provide a detailed characterization of glyoxal oxidation with varying equivalence ratio at a nominal temperature of 603 K. At this intermediate temperature, $HO_2$ related oxidation reactions such as OCHCHO + $HO_2$ become important. However, we were not able to reconcile the results of Hay and Norrish with our present understanding of the reaction system. Using our mechanism, we were able to reproduce qualitatively the product yields and the overall shapes of the experimental concentration−time profiles, but, in fact, they were on a more than 2 orders of magnitude slower time scale. As a possible explanation, the hypotheses of a much higher yield of the OH radical forming channel (R6), OCHCHO + $HO_2$ → HOCHO + CO + OH, was tested. As already stated above and further outlined in the Appendix, we actually recommend the low $k_6$ value calculated by da Silva[34] in our mechanism, which is 2 orders of magnitude smaller than the value reported by Niki et al.[41] In fact, setting $k_6$ to the much higher value of Niki et al. significantly reduces the mismatch of the overall reaction time scales, but the agreement with the reported product yields is seriously deteriorated. In particular, the high yield of $H_2O_2$ reported by Hay and Norrish is considerably underestimated. Further modeling attempts led us to the conclusion that the Hay and Norrish experiments presumably were not performed under isothermal conditions and that the fast observed experimental glyoxal consumption is at least partly due to an unidentified temperature increase of the reaction gas mixture. This uncertainty, along with the issue of potential surface effects in the reactor, makes these data less suitable for kinetic interpretation.

Another test for the glyoxal oxidation mechanism was the modeling of the photolysis experiments of glyoxal/oxygen mixtures performed by Colberg and Friedrichs.[2] Figure 4 shows

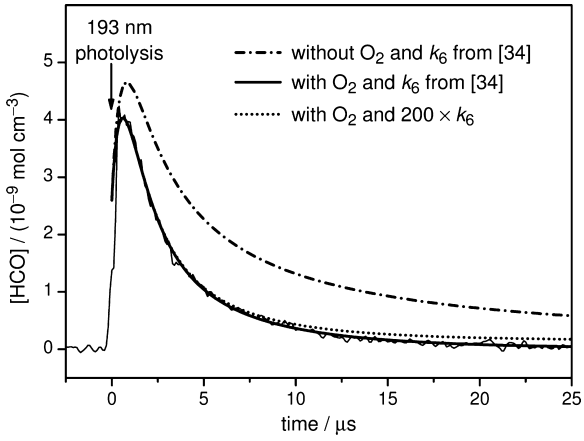


**Figure 4.** Photolysis experiment of Colberg and Friedrichs[2] at $T$ = 857 K and $p$ = 1080 mbar with 2% OCHCHO and 3160 ppm of $O_2$ in the reaction mixture. Three different simulations are shown: without $O_2$ (dash−dotted curve) and with $O_2$ assuming either the rate constant for the reaction OCHCHO + $HO_2$ as reported by Niki et al.[41] (dotted curve) or by da Silva[34] (solid curve).



DOI: 10.1021/jp512432q
J. Phys. Chem. A 2015, 119, 7305−7315

a comparison of an original experiment at $T$ = 857 K taken from ref 2 with simulations of HCO concentration−time profiles with (solid curve) and without oxygen (dash−dotted curve) present in the reaction mixture. Oxygen addition significantly reduces the overall HCO yield and lifetime. The simulation is in perfect agreement with the experimental data. To further investigate the possibility of a significant OH-forming channel of the reaction OCHCHO + $HO_2$, a simulation with the rate of reaction (R6) increased to the Niki et al. value, $k_6 \times 200$, is shown as well (dotted curve). With $k_6 \times 200$, the influence of reaction (R6) on the HCO concentration profile is negligible at short reaction times, but a factor of 4 higher HCO concentration is simulated at $t$ = 25 $\mu$s. In this case, the simulated residual HCO concentration at long reaction times can be traced back to a steady regeneration of HCO radicals due to the combined reaction sequence (R5) and (R10), OCHCHO + OH → HCO + CO + $H_2O$. However, none of the original experiments of Colberg and Friedrichs showed this small but significant HCO concentration plateau at longer reaction times, further supporting the low OH yield from the reaction OCHCHO + $HO_2$, as predicted by da Silva and recommended by us.

## CONCLUSIONS

A detailed glyoxal decomposition and oxidation mechanism has been compiled from literature data merging previous reports on glyoxal/oxygen photolysis at room and high temperature,[19] the branching ratios of glyoxal thermal decomposition,[2] and theoretical studies on the reaction of glyoxal + $HO_2$,[34] OCHCO + $O_2$,[35] and formic acid oxidation.[26]

All HCO profiles from glyoxal decomposition behind shock waves could be very well-simulated, both in terms of absolute HCO concentrations and signal shapes, using the glyoxal decomposition mechanism adopted from Colberg and Friedrichs[2] with branching fractions taken from Friedrichs et al.[19] The established glyoxal pyrolysis mechanism was able to predict the measured HCO concentration−time profiles of this work without any modifications. Moreover, by adding oxygen to the reaction mixtures, the rate constant for the reaction HCO + $O_2$ could be measured at temperatures 1285 K ≤ $T$ ≤ 1705 K, hence significantly extending the range of direct measurements toward higher temperatures. The results are in striking agreement with the previous shock tube/photolysis experiments of Colberg and Friedrichs.[2] The absolute values as well as the overall temperature dependence, which is stronger than predicted theoretically, could be confirmed.

A detailed reanalysis of previous experimental measurements on the reaction OCHCHO + $HO_2$ performed by Niki et al.[41] led us to the conclusion that the reported high OH yield can be traced back to a previously unidentified formation of the recombination product HOCH(OO)CHO and its secondary reaction with $HO_2$. The theoretically predicted, 2 orders of magnitude lower rate constant value for OH formation reported by da Silva[34] is also supported by a reassessment of the previous glyoxal/$O_2$ photolysis data from Colberg and Friedrichs.[2] Using the original high rate constant value of Niki et al., our glyoxal oxidation mechanism would predict HCO concentration plateau levels at long reaction times that have not been observed in the experiment.

Unfortunately, a further critical test of the performance of our mechanism at intermediate temperatures by comparing model predictions with the outcome of the glyoxal oxidation batch reactor experiments of Hay and Norrish[21] turned out to be unfeasible. Most probably, those experiments were biased by an unidentified temperature increase in the reactor. Therefore, additional measurements of glyoxal oxidation at intermediate temperatures are desirable and would offer a possibility to critically check the predicted important role of the reaction OCHCHO + $HO_2$ for the overall reaction progress.

## APPENDIX

### On the OCHCHO + $HO_2$ Reaction

As discussed above, the reaction of OCHCHO with $HO_2$ is believed to be of importance for the generation of chain carriers in oxidation of glyoxal. Figure 5 compares the available rate constant data for the rate of OCHCHO + $HO_2$. According to the recent theoretical study by da Silva,[34] glyoxal reacts with $HO_2$ to form a hydroxyperoxy radical. At low temperatures, the major reaction product is predicted to be collisionally deactivated HOCH(OO)CHO (R7), but a secondary product channel yielding HOCHO and OH

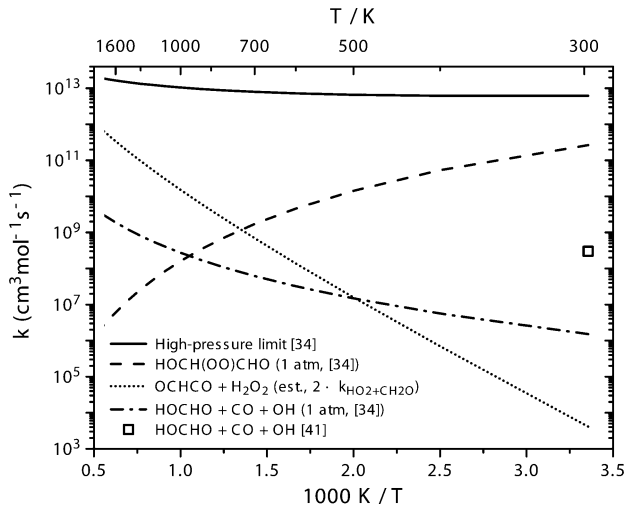


**Figure 5.** Arrhenius plot for the reaction OCHCHO + $HO_2$ → products. The curves denote the rate constants predicted theoretically by da Silva[34] for the total reaction at the high-pressure limit and for the recombination reaction (R6) as well as the OH-producing channel (R7) at 1.0 atm. The H-abstraction channel forming OCHCO + $H_2O_2$ (R8) is an estimate by analogy to the reaction $CH_2O$ + $HO_2$. The square symbol denotes the experimental result for the OH-producing channel (R7) by Niki et al.[41]

$$\text{OCHCHO} + HO_2 \rightarrow \text{HOCHO} + \text{CO} + \text{OH} \qquad \text{(R7)}$$

has been proposed in earlier studies of glyoxal oxidation. The only experimental determination of the rate constant for the OH channel was reported by Niki et al.,[41] who derived a value more than 2 orders of magnitude larger than the theoretical estimate for $k_7$ by da Silva.[34] Figure 5 compares their value (open square) with the theoretical prediction of the rate constants for the different channels of the reaction OCHCHO + $HO_2$.

Due to the importance of the reaction of glyoxal with $HO_2$, it is worthwhile to take a closer look at the experimental results from Niki et al. that form the basis of their estimation of $k_7$. They conducted Cl-atom initiated oxidation studies of glyoxal oxidation, photolyzing a system of $Cl_2$ (100 ppm), OCHCHO (8−22 ppm), $O_2$ (93.3 mbar), and $H_2$ (840 mbar). The following sequence of reactions was intended to provide data


DOI: 10.1021/jp512432q
J. Phys. Chem. A 2015, 119, 7305−7315

on $k_7$: $Cl_2 + h\nu \rightarrow Cl + Cl$, $Cl + H_2 \rightarrow HCl + H$, $H + O_2$ (+M) $\rightarrow HO_2$ (+M), $OCHCHO + HO_2 \rightarrow HOCHO + CO + OH$ (R7), along with the side reaction $HO_2 + HO_2 \rightarrow H_2O_2 + O_2$. Niki et al. used continuous UV light for 60 or 120 s to obtain sufficient photolysis of $Cl_2$. The results of the experiments are shown in Table 5. Results obtained for longer reaction times

**Table 5. Cl-Atom Initiated Reaction in the OCHCHO/$H_2$/$O_2$ System[a]**

| | | | |
|---|---|---|---|
| $[OCHCHO]_0$ (ppm) | 8.5 | 9.0 | 22.4 |
| Irradiation time (s) | 60 | 60 | 120 |
| −Δ[OCHCHO] (ppm) | 0.68 (0.83) | 0.71 (0.88) | 2.14 (3.5) |
| [HCl] (ppm) | 13.4 (12.6) | 12.3 (12.6) | 22.6 (21.4) |
| [HOCHO] (ppm) | 0.34 (0.29) | 0.40 (0.31) | 1.9 (1.2) |
| [CO] (ppm) | 0.90 (0.70) | 1.05 (0.74) | 4.55 (3.0) |
| $[CO_2]$ (ppm) | 0.22 (0.10) | 0.17 (0.10) | 0.53 (0.42) |
| $[H_2O_2]$ (ppm) | 4.9 (6.0) | 5.4 (6.0) | 10.5 (9.6) |

[a]Photolysis of a mixture of $Cl_2$ (100 ppm), OCHCHO (8-22 ppm), $O_2$ (70 Torr), and $H_2$ (630 Torr). Experimental data are from Niki et al.,[41] and modeling results (shown in parentheses) are from the present work.

are neglected here, as Niki et al. reported a considerable loss of species by surface reactions. Niki et al. estimated the $HO_2$ radical concentration from the equation

$$\Delta[H_2O_2] = 2k_{HO_2+HO_2}[HO_2]^2 \times \Delta t$$

using the measured $H_2O_2$ concentration. Then, they calculated the rate constant for (R7) from

$$\Delta[OCHCHO] = k_7[OCHCHO]_{average}[HO_2] \times \Delta t$$

deriving a room temperature of $k_7 = 3 \times 10^8$ cm$^3$ mol$^{-1}$ s$^{-1}$ (Figure 5).

An up-to-date kinetic analysis of the system supports most of the assumptions made by Niki et al. Once formed by the sequence of reactions outlined by Niki et al., $HO_2$ reacts with glyoxal

$$OCHCHO + HO_2 \rightarrow \text{products}$$

or with itself

$$HO_2 + HO_2 \rightarrow H_2O_2 + O_2$$

The major shortcoming of their analysis is the disregard of the formation of HOCH(OO)CHO, which, according to da Silva, is the dominating product of the glyoxal + $HO_2$ reaction. Provided the HOCH(OO)CHO adduct has a sufficiently long lifetime, this adduct may react with $HO_2$ in a secondary reaction. There are no experimental or theoretical data available for HOCH(OO)CHO + $HO_2$, but, from analogy with other hydrocarbon peroxide radicals, the reaction is likely to have two product channels

$$HOCH(OO)CHO + HO_2 \rightarrow HOCH(O)CHO + O_2 + OH \quad \text{(R13)}$$

$$HOCH(OO)CHO + HO_2 \rightarrow HOCH(OOH)CHO + O_2 \quad \text{(R14)}$$

Dissociation of HOCH(O)CHO to HOCHO and HCO is 59 kJ mol$^{-1}$ exothermic. A DFT estimate indicates a barrier to dissociation of merely +1.0 kJ mol$^{-1}$, which drops to −5.0 kJ mol$^{-1}$ at the CBS-QB3 level of theory, so we believe that dissociation of HOCH(O)CHO is essentially instant, even at 298 K. For similar reactions of $HOCH_2OO$, $CH_3C(O)OO$, and $CH_3C(O)CH_2OO$ with $HO_2$, branching fractions $k_{OH}/k_{total}$ of 40%(±25%) have been reported.[54−56] In the present work, we have assumed a branching fraction for HOCH(OO)CHO + $HO_2$ of 50%, together with an overall rate constant of $k_{13+14} = 6.0 \times 10^{12}$ cm$^3$ mol$^{-1}$ s$^{-1}$, which is typical for this type of reaction.

Modeling of the experimental data from Niki et al. with the detailed reaction mechanism of the present work have been performed. Appropriate reactions of chlorine species have been added, and the photolysis rate for $Cl_2$ was fitted such that the calculated concentration of HCl after 60 or 120 s matched reasonably the measured values. The results are shown (in parentheses) in Table 5. Even though we employ a rate constant for $k_7$, which is about 2 orders of magnitude lower than derived by Niki et al., the agreement between measured and predicted concentrations is acceptable. In support of the present interpretation of the reaction system, Niki et al. reported the detection of a transient component, which they believed to be HOCH(OOH)CHO.

## ■ ASSOCIATED CONTENT

### Supporting Information

Detailed glyoxal oxidation reaction mechanism in CHEMKIN format and pressure-dependent rate constant data in PLOG format. This material is available free of charge via the Internet at http://pubs.acs.org.

## ■ AUTHOR INFORMATION


### Corresponding Author

*E-mail: friedrichs@phc.uni-kiel.de.


### Notes

The authors declare no competing financial interest.

## ■ ACKNOWLEDGMENTS

G.F. acknowledges financial support from the Cluster of Excellence *The Future Ocean* at Kiel University and continued sponsorship of the shock tube experiments by the German Science Foundation (DFG-FR 1529/3 and 1529/4). P.M. thanks the Robert A. Welch Foundation (grant B-1174) and the UNT Faculty Research Fund for support.

## ■ REFERENCES


(1) Wang, Q.; Geng, C.; Lu, S.; Chen, W.; Shao, M. Emission factors of gaseous carbonaceous species from residential combustion of coal and crop residue briquettes. *Front. Environ. Sci. Eng.* **2013**, *7*, 66−76.

(2) Colberg, M.; Friedrichs, G. Room temperature and shock tube study of the reaction HCO + $O_2$ using the photolysis of glyoxal as an efficient HCO source. *J. Phys. Chem. A* **2006**, *110*, 160−170.

(3) Calvert, J. G.,; Atkinson, R.; Becker, K. H.; Kamens, R. H.; Seinfeld, J. H.; Wallington, T. J.; Yarwoog, G. *The Mechanism of Atmospheric Oxidation of Aromatic Hydrocarbons*; Oxford University Press: Oxford, 2000.

(4) Stavrakou, T.; Müller, J.-F.; De Smedt, I.; Van Roozendael, M.; Kanakidou, M.; Vreskoussis, M.; Wittrock, F.; Richter, A.; Burrows, J. P. The continental source of glyoxal estimated by the synergistic use of spaceborne measurements and inverse modelling. *Atmos. Chem. Phys.* **2009**, *9*, 8431−8446.

(5) Hay, J. M.; Norrish, R. G. W. The oxidation of gaseous glyoxal. *Proc. R. Soc. London, Ser. A* **1965**, *288*, 17−38.

(6) Stevenson, T. M.; Tipper, C. F. H. The photoinduced oxidation of acetylene. *Combust. Flame* **1967**, *11*, 35−48.




DOI: 10.1021/jp512432q
J. Phys. Chem. A 2015, 119, 7305−7315

(7) Hay, J. M.; Lyon, D. Alkyne oxidation. I. Acetylene oxidation. *Proc. R. Soc. London, Ser. A* **1970**, *317*, 1−20.
(8) Williams, A.; Smith, D. B. Combustion and oxidation of acetylene. *Chem. Rev.* **1970**, *70*, 267−293.
(9) Alzueta, M. U.; Borruey, M.; Callejas, A.; Millera, A.; Bilbao, R. An experimental and modeling study of the oxidation of acetylene in a flow reactor. *Combust. Flame* **2008**, *152*, 377−386.
(10) Siese, M.; Zetzsch, C. Addition of OH to acetylene and consecutive reactions of the adduct with $O_2$. *Z. Phys. Chem.* **1995**, *188*, 75−89.
(11) Bohn, B.; Zetzsch, C. Formation of $HO_2$ from OH and $C_2H_2$ in the presence of $O_2$. *J. Chem. Soc., Faraday Trans.* **1998**, *94*, 1203−1210.
(12) Yeung, L. Y.; Pennino, M. J.; Miller, A. M.; Elrod, M. J. Kinetics and mechanistic studies of the atmospheric oxidation of alkynes. *J. Chem. Phys. A* **2005**, *109*, 1879−1889.
(13) Maranzana, A.; Ghigo, G.; Tonachini, G.; Barker, J. R. Tropospheric oxidation of ethyne and but-2-yne. 1. Theoretical mechanistic study. *J. Chem. Phys. A* **2008**, *112*, 3656−3665.
(14) Galano, A.; Ruiz-Suarez, L. G.; Vivier-Bunge, A. On the mechanism of the OH initiated oxidation of acetylene in the presence of $O_2$ and $NO_x$. *Theor. Chem. Acc.* **2008**, *121*, 219−225.
(15) Glowacki, D. R.; Lockhart, J.; Blitz, M. A.; Klippenstein, J.; Pilling, M. J.; Robertson, S. H.; Seakins, P. W. Interception of excited vibrational quantum states by $O_2$ in atmospheric association reactions. *Science* **2012**, *337*, 1066−1069.
(16) Lockhart, J.; Blitz, M. A.; Heard, D. E.; Seakins, P. W.; Shannon, R. J. Mechanism of the reaction of OH with alkynes in the presence of oxygen. *J. Chem. Phys. A* **2013**, *117*, 5407−5418.
(17) Steacie, E. W. R.; Hatcher, W. H.; Horwood, J. F. Kinetics of the decomposition of gaseous glyoxal. *J. Chem. Phys.* **1935**, *3*, 291−295.
(18) Saito, K.; Kakumoto, T.; Murakami, I. Thermal unimolecular decomposition of glyoxal. *J. Phys. Chem.* **1984**, *88*, 1182−1187.
(19) Friedrichs, G.; Colberg, M.; Dammeier, J.; Bentz, T.; Olzmann, M. HCO formation in the thermal unimolecular decomposition of glyoxal: rotational and weak collision effects. *Phys. Chem. Chem. Phys.* **2008**, *10*, 6520−6533.
(20) Steacie, E. W. R.; Hatcher, W. H.; Horwood, J. F. The kinetics of the oxidation of gaseous glyoxal. *J. Chem. Phys.* **1935**, *3*, 551−555.
(21) Hay, J. M.; Norrish, R. G. W. The oxidation of gaseous glyoxal. *Proc. R. Soc. London, Ser. A* **1965**, *288*, 1−16.
(22) Hay, J. M. The competitive oxidation of formaldehyde and glyoxal. *J. Chem. Soc.* **1965**, *8*, 7388−7391.
(23) Newitt, D. M.; Baxt, L. M.; Kelkar, V. V. The oxidation of aldehydes. Part I. The combustion zones of butaldehyde, isobutaldehyde, propaldehyde, acetaldehyde, glyoxal, and acraldehyde. *J. Chem. Soc.* **1939**, 1703−1710.
(24) Payne, J. H.; Lemon, G. F., Jr. The oxidation of aldehydes with hydrogen peroxide. *J. Am. Chem. Soc.* **1941**, *63*, 226−228.
(25) Thomas, J. H. Gas-phase reactions of nitrogen dioxide. Part 2 - The oxidation of glyoxal. *Trans. Faraday Soc.* **1953**, *49*, 630−635.
(26) Marshall, P.; Glarborg, P. Ab initio and kinetic modeling studies of formic acid oxidation. *Proc. Combust. Inst.* **2015**, *35*, 153−160.
(27) Friedrichs, G.; Davidson, D. F.; Hanson, R. K. Validation of a thermal decomposition mechanism of formaldehyde by detection of $CH_2O$ and HCO behind shock waves. *Int. J. Chem. Kinet.* **2004**, *36*, 157−169.
(28) Rasmussen, C. L.; Hansen, J.; Marshall, P.; Glarborg, P. Experimental measurements and kinetic modeling of $CO/H_2/O_2/NO_x$ conversion at high pressure. *Int. J. Chem. Kinet.* **2008**, *40*, 454−480.
(29) Hashemi, H.; Christensen, J. M.; Gersen, S.; Glarborg, P. Hydrogen oxidation at high pressure and intermediate temperatures: experiments and kinetic modeling. *Proc. Combust. Inst.* **2015**, *35*, 553−560.
(30) Burcat, A.; Ruscic, B. *Third Millennium Ideal Gas and Condensed Phase Thermochemical Database for Combustion with Updates from Active Thermochemical Tables*; Argonne National Laboratory: Argonne, IL, 16th September, 2005; Report ANL-05/20.
(31) Montgomery, J. A., Jr.; Frisch, M. J.; Ochterski, J. W.; Petersson, G. A. A complete basis set model chemistry. VI. Use of density functional geometries and frequencies. *J. Chem. Phys.* **1999**, *110*, 2822−2827.
(32) Feierabend, K. J.; Zhu, L.; Talukdar, R. K.; Burkholder, J. B. Rate coefficients for the OH + HC(O)C(O)H (glyoxal) reaction between 210 and 390 K. *J. Phys. Chem. A* **2008**, *112*, 73−82.
(33) Lockhart, J.; Blitz, M.; Heard, D.; Seakins, P.; Shannon, R. Kinetic study of the OH + glyoxal reaction: experimental evidence and quantification of direct OH recycling. *J. Phys. Chem. A* **2013**, *117*, 11027−11037.
(34) da Silva, G. Kinetics and mechanism of the glyoxal + $HO_2$ reaction: conversion of $HO_2$ to OH by carbonyls. *J. Phys. Chem. A* **2011**, *115*, 291−297.
(35) da Silva, G. Hydroxyl radical regeneration in the photochemical oxidation of glyoxal: kinetics and mechanism of the HC(O)CO + $O_2$ reaction. *Phys. Chem. Chem. Phys.* **2010**, *12*, 6698−6705.
(36) Hsu, C.-C.; Mebel, M.; Lin, M. C. Ab initio molecular orbital study of the HCO + $O_2$ reaction: direct versus indirect abstraction channels. *J. Chem. Phys.* **1996**, *105*, 2346−2352.
(37) Koch, D. M.; Khieu, N. H.; Peslherbe, G. H. Ab initio studies of the glyoxal unimolecular dissociation pathways. *J. Phys. Chem. A* **2001**, *105*, 3598−3604.
(38) Hepburn, J. W.; Buss, R. J.; Butler, L. J.; Lee, Y. T. Molecular beam study of the photochemistry of $S_1$ glyoxal. *J. Phys. Chem.* **1983**, *87*, 3638−3641.
(39) Plum, C. N.; Sanhueza, E.; Atkinson, R.; Carter, W. P. L.; Pitts, J. N. Hydroxyl radical rate constants and photolysis rates of $\alpha$-dicarbonyls. *J. Environ. Sci. Technol.* **1983**, *17*, 479−484.
(40) Galano, A.; Alvarez-Idaboy, J. R.; Ruiz-Santoyo, M. E.; Vivier-Bunge, A. Mechanism and kinetics of the reaction of OH radicals with glyoxal and methylglyoxal: a quantum chemistry + CVT/SCT approach. *ChemPhysChem* **2004**, *5*, 1379−1388.
(41) Niki, H.; Maker, P. D.; Savage, C. M.; Breitenbach, L. P. An FTIR study of the chlorine-atom-initiated reaction of glyoxal. *Int. J. Chem. Kinet.* **1985**, *17*, 547−558.
(42) Orlando, J. J.; Tyndall, G. S. The atmospheric chemistry of the HC(O)CO radical. *Int. J. Chem. Kinet.* **2001**, *33*, 149−156.
(43) Friedrichs, G.; Herbon, J. T.; Davidson, D. F.; Hanson, R. K. Quantitative detection of HCO behind shock waves: The thermal decomposition of HCO. *Phys. Chem. Chem. Phys.* **2002**, *4*, 5778−5788.
(44) Friedrichs, G. Sensitive absorption methods for quantitative gas phase kinetic measurements. Part 1: Frequency Modulation Spectroscopy. *Z. Phys. Chem.* **2008**, *222*, 1−30.
(45) Flad, J. E.; Brown, S. S.; Burkholder, J. B.; Stark, H.; Ravishankara, A. R. Absorption cross sections for the $\tilde{A}\ ^2A''\ (0,9^0,0) \leftarrow \tilde{X}\ ^2A'\ (0,0^1,0)$ band of the HCO radical. *Phys. Chem. Chem. Phys.* **2006**, *8*, 3636−3642.
(46) Friedrichs, G.; Colberg, M.; Fikri, M.; Huang, Z.; Neumann, J.; Temps, F. Validation of the extended simultaneous kinetics and ringdown model by measurements of the reaction $NH_2$ + NO. *J. Phys. Chem. A* **2005**, *109*, 4785−4795.
(47) Millikan, R. C.; White, D. R. Vibrational energy exchange between $N_2$ and CO. The vibrational relaxation of nitrogen. *J. Chem. Phys.* **1963**, *39*, 98−101.
(48) Kee, R. J.; Rupley, F. M.; Miller, J. A. *Chemkin II: A Fortran Chemical Kinetics Package for the Analysis of Gas Phase Chemical Kinetics*; Sandia National Laboratories: Livermore, CA, 1989; Report SAND89-8009.
(49) Lutz, A. E.; Kee, R. J.; Miller, J. A. *Senkin: A Fortran Program for Predicting Homogeneous Gas Phase Chemical Kinetics with Sensitivity Analysis*; Sandia National Laboratories: Livermore, CA, 1990; Report SAND87-8248.
(50) DeSain, J. D.; Jusinski, L. E.; Ho, A. D.; Taatjes, C. A. Temperature dependence and deuterium kinetic isotope effects in the HCO (DCO) + $O_2$ reaction between 296 and 673 K. *Chem. Phys. Lett.* **2001**, *347*, 79−86.
(51) Smith, G. P.; Golden, D. M.; Frenklach, M.; Moriarty, N. W.; Eiteneer, B.; Goldenberg, M.; Bowman, C. T.; Hanson, R. K.; Song, S.; Gardiner, W. C., Jr.; Lissianski V., Qin, Z. *GRI-Mech*, version 3.0, 1999; http://www.me.berkeley.edu/gri_mech (accessed 15. Jan. 2015).


DOI: 10.1021/jp512432q
*J. Phys. Chem. A* 2015, 119, 7305−7315

(52) Veyret, B.; Lesclaux, R. Absolute rate constants for the reactions of the formyl radical HCO with oxygen and nitric oxide from 298 to 503 K. *J. Phys. Chem.* **1981**, *85*, 1918−1922.
(53) Timonen, R. S.; Ratajczak, E.; Gutman, D. Kinetics of the reactions of the formyl radical with oxygen, nitrogen dioxide, chlorine, and bromine. *J. Phys. Chem.* **1988**, *92*, 651−655.
(54) Hasson, A. S.; Tyndall, G. S.; Orlando, J. J. A product yield study of the reaction of $HO_2$ radicals with ethyl peroxy ($C_2H_5O_2$), acetyl peroxy ($CH_3C(O)O_2$), and acetonyl peroxy ($CH_3C(O)CH_2O_2$) radicals. *J. Phys. Chem. A* **2004**, *108*, 5979−5989.
(55) Jenkin, M. E.; Hurley, M. D.; Wallington, T. J. Investigation of the radical product channel of the $CH_3COO_2$ + $HO_2$ reaction in the gas phase. *Phys. Chem. Chem. Phys.* **2007**, *9*, 3149−3162.
(56) Jenkin, M. E.; Hurley, M. D.; Wallington, T. J. Investigation of the radical product channel of the $CH_3C(O)CH_2O_2$ + $HO_2$ reaction in the gas phase. *Phys. Chem. Chem. Phys.* **2008**, *10*, 4274−4280.



DOI: 10.1021/jp512432q
*J. Phys. Chem. A* 2015, 119, 7305−7315